JOURNAL OF GEOPHYSICAL RESEARCH, VOL. 112, B10209, doi:10.1029/2004JB003213, 2007

Direct simulation of fluid-solid mechanics in porous media using the discrete element and lattice-Boltzmann methods

David F. Boutt,[1] Benjamin K. Cook,[2] Brian J. O. L. McPherson,[3] and J. R. Williams[4]

Received 4 June 2004; revised 11 June 2007; accepted 16 July 2007; published 24 October 2007.

[1] A detailed understanding of the coupling between fluid and solid mechanics is important for understanding many processes in Earth sciences. Numerical models are a popular means for exploring these processes, but most models do not adequately handle all aspects of this coupling. This paper presents the application of a micromechanically based fluid-solid coupling scheme, lattice-Boltzmann discrete element method (LBDEM), for porous media simulation. The LBDEM approach couples the lattice-Boltzmann method for fluid mechanics and a discrete element method for solid mechanics. At the heart of this coupling is a previously developed boundary condition that has never been applied to coupled fluid-solid mechanics in porous media. Quantitative comparisons of model results to a one-dimensional analytical solution for fluid flow in a slightly deformable medium indicate a good match to the predicted continuum-scale fluid diffusion-like profile. Coupling of the numerical formulation is demonstrated through simulation of porous medium consolidation with the model capturing poroelastic behavior, such as the coupling between applied stress and fluid pressure rise. Finally, the LBDEM model is used to simulate the genesis and propagation of natural hydraulic fractures. The model provides insight into the relationship between fluid flow and propagation of fractures in strongly coupled systems. The LBDEM model captures the dominant dynamics of fluid-solid micromechanics of hydraulic fracturing and classes of problems that involve strongly coupled fluid-solid behavior.

Citation: Boutt, D. F., B. K. Cook, B. J. O. L. McPherson, and J. R. Williams (2007), Direct simulation of fluid-solid mechanics in porous media using the discrete element and lattice-Boltzmann methods, *J. Geophys. Res.*, *112*, B10209, doi:10.1029/2004JB003213.

1. Introduction

[2] Fundamental problems in geology and geological engineering commonly involve analysis of coupled processes in heterogeneous systems, such as thermomechanical, hydromechanical, and chemomechanical processes. Analysis and interpretation of coupled problems typically rely on more sophisticated conceptual models and have more degrees of freedom than uncoupled problems [*Yow and Hunt*, 2002]. Our long-term goal is to understand the dynamics of coupled fluid-solid processes in hydrogeology and geomechanics. One example is the generation of deep subsurface rock fractures by anomalous fluid pressures. In sedimentary basins, fluid pressures may be elevated by many different processes [see *Neuzil*, 1995] and attain large magnitudes relative to hydrostatic, sometimes exceeding the least principal stress [*McPherson and Bredehoeft*, 2001]. The rate of pressure dissipation is governed by rock hydraulic diffusivity and the rate of pressure generation. Macroscopic (i.e., continuum) descriptions of these processes typically yield first-order controls on system behavior, but do not address smaller-scale processes responsible for observed inelastic rock deformation. Of particular importance are the initiation and propagation of extension fractures and associated feedbacks between the fluid flow field and the mechanical state of the rock. A detailed understanding of the coupled pore-scale physics facilitates improved interpretation and reduction of field data and experimental results.

[3] Problems involving coupled processes are typically addressed with continuum models that rely on constitutive relations developed through experimental work [*Neuzil*, 2003]. Unfortunately, continuum models typically yield little insight into underlying material micromechanics and do not allow the identification of important subcontinuum material properties. Another approach to understanding coupled processes is to use a discrete mechanical approach that controls and tracks additional (micromechanical) parameters, including pore structure, such as the discrete element method (DEM). An advantage of using DEM models for solid mechanics is that the underlying physics are clearly resolved and the models are

[1]Department of Geosciences, University of Massachusetts Amherst, Amherst, Massachusetts, USA.
[2]Infrastructure and Information Technology, Sandia National Laboratories, Albuquerque, New Mexico, USA.
[3]Department of Civil and Environmental Engineering, University of Utah, Salt Lake City, Utah, USA.
[4]Department of Civil and Environmental Engineering, Massachusetts Institute of Technology, Cambridge, Massachusetts, USA.

0148-0227/07/2004JB003213$09.00

inherently discontinuous and heterogeneous. In this paper we apply a coupled model [*Cook et al.*, 2000; *Cook*, 2001; *Cook et al.*, 2004] that uses the DEM for resolving solid mechanics and the lattice-Boltzmann method (LB) to simulate fluid mechanics. LB is an efficient method for solving the Navier-Stokes equations of incompressible fluid flow. The solid and fluid mechanics are resolved by simulating flow at the pore-scale and computing fluid-grain coupling. Implicit assumptions about effective stress and continuum-scale porosity-permeability relationships are not necessary, because the solid framework is made of discrete elements. Their deformation and movement will directly change porosity and hence permeability of the system. Continuum-scale constitutive relations, between porosity and permeability, can be considered results rather than assumptions.

[4] Coupling between fluids and solids in porous medium results from direct interaction in pores. For instance, as the volume of a pore space collapses, fluid is forced to either compress or flow out of the pore. Conversely, a fluid pressure change imparts a tangible force on the solid grain walls of the pore. This microscale interaction is the most fundamental feedback loop (coupling) in the mechanics of saturated porous media. On a macroscopic scale, coupling between fluids and solids result from changes in pore-space (mechanical to fluid) and/or changes in effective stress (fluid to mechanical). In this work we take a micromechanical approach to the fluid-solid coupling problem by applying the direct simulation approach developed by *Cook* [2001] and *Cook et al.* [2004] to porous media. Continuum-scale relations are not used to relate fluid flux to pressure drop at the pore scale, rather assumptions of pore-scale physics are employed. Also, because the model directly simulates movement and deformation of the solid matrix, no assumptions about the continuum-scale relationship between fluid permeability and porosity are necessary. The hydrodynamics evolve with the changing solid matrix.

[5] Using the lattice-Boltzmann discrete element method (LBDEM) model, we simulate unsteady fluid flow through nonstationary discrete media. A quantitative comparison to a one-dimensional (1-D) analytical solution for fluid flow in a slightly deformable medium is presented. Phenomena captured and verified include the compressible storage of porous media and the resulting transience of fluid flow. Simulations of porous medium consolidation were compared to results predicted by poroelasticity theory. Comparison of model results to the classic Terzaghi consolidation problem enables the analysis and determination of the sensitivity of key model parameters to explore controls on poroelastic behavior of the model. Additionally, the model is applied to study the genesis and propagation of natural hydraulic fractures, an application in which strong coupling between fluid pressure and solid mechanics exists. The model simulates the generation of extension fractures, fracture propagation, and the interaction between fractures and fluid flow. Results from these simulations suggest that fluid forcing on the scale of the sample is a significant contributor to sample deformation.

2. Modeling Approach

[6] This work investigates hydromechanical behavior of porous media using a DEM technique for solid mechanics first presented by *Cundall* [1971] and *Cundall and Strack* [1979], which has successfully approximated the behavior of noncohesive, granular systems under low stress conditions [*Cundall et al.*, 1982; *Cleary and Campbell*, 1993; *Campbell et al.*, 1995; *Morgan*, 1999; *Morgan and Boettcher*, 1999], and lithified sedimentary rocks [*Bruno and Nelson*, 1991; *Potyondy et al.*, 1996; *Hazzard et al.*, 2000; *Boutt and McPherson*, 2002]. Extensive comparisons of the DEM to theoretical, numerical, and experimental systems have been performed [*Pande et al.*, 1990]. For fluid mechanics we use the LB method [*Chen and Doolen*, 1998] a Navier-Stokes based numerical technique which uses lattice-gas theory to approximate the equations of incompressible fluid flow. Although *Cook et al.* [2004] presents extensive validations of the coupling of the codes for single and few particle systems, the application of the coupling technique to porous media type flows has not been demonstrated, tested, or applied.

2.1. Discrete Element Method

[7] In this paper we use a traditional DEM approach similar to that presented by *Cleary and Campbell* [1993]; *Campbell et al.* [1995]; *Morgan* [1999]; *Morgan and Boettcher* [1999], based on an existing two-dimensional DEM application [*Rege*, 1996; *Williams and Rege*, 1997]. (The coupled LBDEM, originally called Modeling Interacting Multibody Engineering Systems (MIMES [*Rege*, 1996]) was developed jointly by MIT (J. Williams, PI) and Sandia National Laboratories (D. Preece, PI; B. Cook, PI) through a multiyear collaboration funded in part by the U.S. Department of Energy. *Cook* [2001] highlights the addition of the lattice-Boltzmann method to and an extension of the MIMES framework through funding provided by the National Oil and Gas Technology Partnership (NGOTP).) Verification problems for the code used in this paper is given by *Rege* [1996]. DEM simulates the mechanical behavior of porous media by idealizing the system as a collection of separate particles that interact at their contact points. The method consists of identifying elements in contact and then resolving the contact physics. The calculations performed in DEM alternate between the application of Newton's second law and a force-displacement law (simple contact model) at the contacts between particles. The force-displacement law relates components of force to corresponding components of relative displacements through a generalized contact constitutive model. Normal displacements between adjoining elements result in local overlaps that are small compared to the overall length scale of the element. The contact constitutive model applied comprises a stiffness model and a slip model. The motion equations are then integrated explicitly with respect to time to obtain particle positions. Positions at each time step are then used in force-displacement calculations and the calculation cycle starts over again. The basic theory of DEM and its methods is given by *Pande et al.* [1990]. DEM constitutive behaviors, including stress and strain relations, are results rather than implicit constitutive assumptions.

2.2. Lattice-Boltzmann and Coupled Model Theory

[8] Fluid coupling with DEM was developed by *Cook* [2001] and *Cook et al.* [2004] through explicit integration of

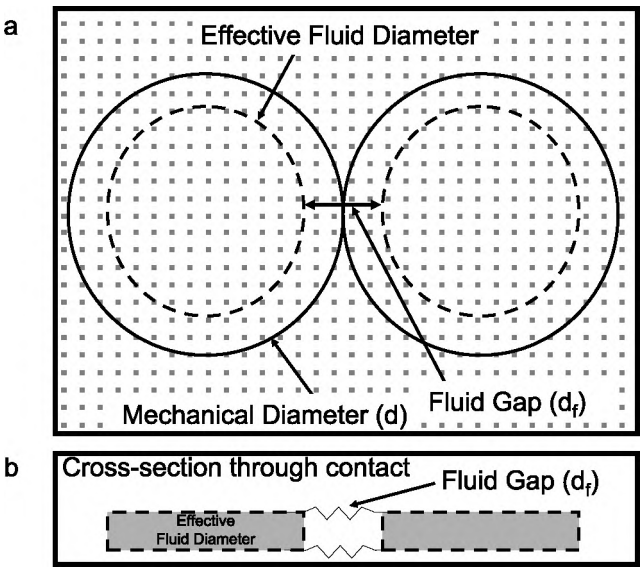

Figure 1. Schematic of two-dimensional approximation for fluid flow through a compact assembly of discrete elements. (a) Fluid pathways are simulated by employing a smaller hydraulic radius (dashed lines) than the radius used to define mechanical elements (solid lines). Squares depict lattice nodes for lattice-Boltzmann fluid flow calculation. (b) A cross section through the contact can be envisioned as a two unit thickness elements separated by springs which allow fluid to pass through unobstructed.

an LB algorithm with the DEM framework described above. Details of Cook's coupling approach is reviewed by *Cook et al.* [2004]. The velocity of the fluid is set to maintain the no-slip boundary condition on the solid particle. As a result of this condition, a momentum imbalance between the fluid and solid particle arises. This imbalance is resolved through the exchange of momentum between the solid to the fluid, resulting in a net force on the solid. A unique aspect of this coupling scheme is that the fluid is handled in a Eularian sense, where the fluid grid is stationary, while the DEM scheme is Lagrangian and particles actively move across the fluid grid. Therefore discrete elements are tracked relative to the fluid grid by calculating the percentage of fluid nodes covered by solid (termed the solid ratio). The codes are currently weakly coupled and all simulations in this paper use a 1:1 DEM to LB time step unless otherwise noted. The two-dimensional simulations reported by *Cook* [2001] include complex phenomena like drafting-kissing-tumbling in multiparticle sedimentation simulations and the saltation phase of bed erosion.

[9] Detailed testing and evaluation of the coupled code have been performed and are available from *Boutt* [2004] and the auxiliary materials[1]. (See auxiliary materials for more details on model validation and verification.) *Boutt* [2004] and *Boutt et al.* [2003] give an extensive discussion of the effects of LB grid resolution on overall model accuracy. Additionally, comparisons of model results to steady flow problems, such as flow around cylinders and flow through packed assemblies of discs (including comparisons to Darcy's law), yield good results.

2.3. Model Two Dimensionality

[10] The current formulation of the LBDEM consists of a two-dimensional system. Many fundamental problems can still be addressed using two-dimensional models but understanding the limitations of these assumptions is key to successful model application. We are currently limited to a two-dimensional system due to the complexity and the computational overhead of a fully coupled three-dimensional model. Thus initial model development took place with a two-dimensional model and the results of this model applied to coupled fluid flow and deformation in porous media is presented in this paper. A three-dimensional prototype of the LBDEM is currently being developed at Sandia National Laboratories.

[11] In a compacted or very densely packed two-dimensional assembly of discrete elements (such as a rock or sediment), a physically unrealistic situation arises in the form of no connected paths for fluid to flow through. To facilitate the use of two-dimensional fluid coupling for applications in porous media, an assumption about the fluid flow paths is made. This problem has been addressed previously for the case of flow network models [*Bruno and Nelson*, 1991; *Bruno*, 1994; *Li and Holt*, 2001] and continuum Darcy's models [*O'Connor et al.*, 1997]. In both models, fluid is assumed to flow out of plane and around solids. We take a similar approach in that the LB fluid interacts with a percentage of the discrete elements, resulting in a smaller element size used to resolve the fluid through the assembly. Figure 1a illustrates this concept for two discs in contact depicting the mechanical discrete element (d, solid line) and the effective hydraulic diameter (dashed line). The fluid gap (d_f) is be approximated by

$$d_f = 2d(1 - d_h), \tag{1}$$

with d_h defined as a percentage based multiplier for the hydraulic diameter. The hydraulic diameter multiplier (d_h) is treated as an input parameter used to vary the effective hydraulic diameter, the magnitude of d_f, and consequently the initial bulk properties of the porous media. This idealization of the 2-D system for granular and cemented granular material can be thought of as two objects being separated by springs supporting normal and shear force, but not interfering with fluid flow (Figure 1b). In essence, the contact between the discrete elements provides the normal and shear support and the resulting fluid gap defines the geometry for fluid flow. Fluid momentum calculations are based on the effective hydraulic diameter. The fluid gap will vary spatially depending on the relative size of the discrete elements in consideration and the existence or lack thereof contact between the particles. Recall that discrete elements are allowed to overlap a small amount, and thus the effective hydraulic diameter will be reduced when overlap occurs. The magnitude of the overlap of the discrete elements is proportional to the stiffness and force of the contact and for stiff grains, such as sand, the hydraulic diameter reduction will be small (<1%) compared to the grain size. The relationships of model parameters, such as

[1]Auxiliary materials are available in the HTML. doi:10.1029/2004JB003213.

the hydraulic diameter, to three-dimensional quantities are presented in the auxiliary material.

3. Unsteady Flow Through Nonstationary Media

[12] Unsteady fluid flow through nonstationary porous media comprise the majority of problems in encountered in the earth sciences. For example, flow to a shallow groundwater well in a confined aquifer includes elastic deformation of the aquifer material due to fluid pressure changes and converging flow around the wellbore [*Helm*, 1994]. Sources of water provided to the well under pumping conditions include deformation of the aquifer that releases water from storage and expansion of water volume following pressure reduction. We now examine these important phenomena with the coupled LBDEM model. In the problem of 1-D consolidation of a layer of porous media, compaction of the aquifer material results in an increase in fluid pressure that forces fluid out of the formation. Like the problem of flow to a well, elastic deformations of the solid framework and the fluid compressibility act together to influence changes in fluid pressure. In section 3.1, we compare a 1-D analytical solution for fluid flow in a slightly compressible elastic porous medium to LBDEM model simulations. We further compare the LBDEM model to poroelasticity theory using an extension of the analytical solution to a 1-D consolidation problem.

3.1. Fluid Flow in Slightly Compressible Porous Media

[13] We now conduct simulations to examine transient behavior in the LBDEM models and to derive continuum parameters governing fluid flow, such as hydraulic diffusivity, and compare results of these simulations to an analytical solution. In discrete models of porous media, averaged quantities such as permeability and diffusivity are not easily calculated, especially because of their scale dependence. To parameterize a discrete model of porous media, it is necessary to determine "micro" parameters, such as pore throat sizes and bond stiffness, which give rise to the more intuitive "macro" or continuum parameters, such as permeability and bulk modulus. The relationship between continuum parameters and micro parameters for dry rock has been previously examined with DEM models [*Boutt and McPherson*, 2002; *Potyondy and Cundall*, 2004] by comparing laboratory experimental results to numerical simulation results. In section 3.2 we will first calculate macroscopic continuum parameters from poroelasticity theory using uncoupled model behavior and then compare an analytical solution based on the parameterization to the coupled LBDEM.

[14] The governing equation for 1-D fluid flow in an isotropic homogeneous porous media in the absence of body forces is

$$\frac{\partial P}{\partial t} = c\frac{\partial^2 P}{\partial x^2}, \tag{2}$$

where P is fluid pressure, t is time, x is the spatial coordinate, and c is the hydraulic diffusivity. The hydraulic diffusivity can be defined as

$$c = \frac{k}{\mu S}, \tag{3}$$

with the parameter c being a combination of the porous medium's intrinsic permeability, k, and storage capacity, S, (commonly referred to as the uniaxial specific storage, $S = S_s/\rho g$). This is the only material parameter needed to define the transient flow field of an isotropic homogeneous porous medium. The specific storage is one of four properties in the general constitutive poroelastic equations and contains fluid and medium compressibility components [*Green and Wang*, 1990].

[15] The uniaxial specific storage (S) can be further broken down into respective fluid and solid components of porous media by assuming incompressible pores and grains giving

$$S = \frac{1}{K_v} + n\frac{1}{K_f}, \tag{4}$$

where K_v is the uniaxial drained bulk modulus, n is porosity, and K_f is the pore fluid bulk modulus [*Wang*, 2000]. Thus the specific storage under these conditions is a linear combination of the porous media compressibility and the pore fluid compressibility. These parameters are directly obtained (n) or measurable (K_v, K_f) in our model of porous media. The drained bulk modulus is a parameter that relies solely on the DEM formulation whereas the hydraulic conductivity and fluid compressibility are parameters that rely on the fluid model. Combined with an independent measurement of permeability, such as that obtained with a measure of fluid flux, a pressure gradient, and Darcy's Law, it is possible to calculate the value of hydraulic diffusivity for the modeled system.

[16] Analytical solutions for the diffusion equation (2) subject to various boundary conditions and initial conditions are widely available [e.g., *Carslaw and Jaeger*, 1959].

3.2. Transient Fluid Flow Through Porous Media With LBDEM Model

[17] A LBDEM model was built to quantitatively compare modeled results to the analytical solution. An assembly of approximately 1000 ellipse-shaped elements is packed into an 18 cm by 9 cm rectangular region bounded by no-displacement, no-flow walls as shown in Figure 2. No cohesion between elements was applied. The packing procedure consists of generating a uniform distribution (see Table 1 for range of radii) of elements on a regular lattice and letting them settle under gravity. Upon reaching equilibrium, the assembly is confined and released from applied loading and allowed to come to equilibrium once again. The assembly is then loaded via platens to a desired stress state, equivalent to atmospheric pressure at the side boundaries. Physical properties of the discrete elements were assigned to mimic those of quartz grains and are listed in Table 1.

[18] The hydraulic diffusivity was calculated for the model setup using poroelasticity theory with measurements of hydraulic conductivity, bulk modulus, porosity, and pore fluid bulk modulus. Hydraulic conductivity of the sample assembly was measured by applying Darcy's law with a fluid pressure gradient across the sample and measuring fluid discharge. In this measurement solid particles were held in place by fixing velocities of the elements to zero. The drained bulk modulus of the sample was measured by performing a dry uniaxial compression test and interpreting

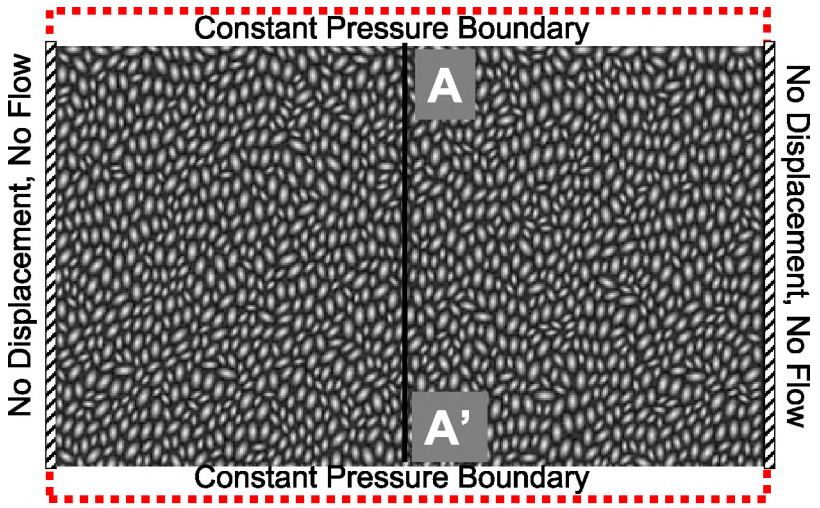

Figure 2. Conceptual model for 1-D fluid flow problem through nonstationary media showing boundary conditions and model geometry. Shaded particles are DEM elements in a black background of fluid. Elements are fully packed in this model, though they appear to be completely separated by fluid. Line A-A′ indicates cross section depicted in Figure 3.

bulk behavior in the context of elasticity theory [*Boutt and McPherson*, 2002]. Pore fluid bulk modulus (inverse of fluid compressibility) is approximated by measuring the pore pressure change of the pure fluid under applied load boundary conditions. *Boutt* [2004] performed this measurement using a small box of fluid with constant load boundary conditions on all sides. All parameters are presented in Table 1, together with the predicted hydraulic diffusivity of the system, which for this model was 8.6 $cm^2\ s^{-1}$.

[19] Because the LBDEM is not a 1-D formulation, it was necessary to apply different boundary conditions to the solids than those to the fluid to facilitate comparison to the 1-D analytical solution. The LBDEM model perpendicular to the flow direction (horizontal in Figure 2) was extended and the boundaries assigned a no-displacement condition for solids and a no-flow condition for fluids. The extension of the boundaries in our LBDEM model is of similar nature to that of applying the solution of equation (2) to fluid flow in an axisymmetric right cylinder. The boundary conditions parallel to the fluid-flow direction (vertical in Figure 2) for the LBDEM model are identical to those for the analytical solution with the solids given a free boundary. The fluid lattice was assigned dimensions of 735 × 401 for a total of 294,735 fluid nodes. The fluid lattice was initialized with a constant pressure of P_o and both boundaries were fixed with a constant pressure of 0 (gauge pressure) during the simulation. The model was executed until the pressure in the pore spaces reached equilibrium with boundary conditions.

[20] One-dimensional cross sections through the model were chosen to compare to the analytical solution. A typical cross section (A-A′ on Figure 2) is plotted in Figure 3,

Table 1. Solid and Fluid Parameters for Transient Fluid Flow and Consolidation Problems[a]

Parameter	Values
Solid	
Friction, dimensionless	0.5
Normal stiffness, dyn cm^{-1}	8.0×10^4
Shear stiffness, dyn cm^{-1}	8.0×10^4
Element size range, cm	0.11–0.07
Fluid radius, dimensionless	0.8
Fluid	
Viscosity, $cm^2\ s^{-1}$)	0.1
Relaxation time, dimensionless	0.875
Node spacing, cm	0.0067
Time step, s	5.5×10^{-5}
Bulk material	
Intrinsic permeability, cm^2	2.4×10^{-5}
Uniaxial drained bulk modulus, dyn cm^{-2}	4.0×10^5
Pore fluid bulk modulus, dyn cm^{-2}	1.6×10^4
Porosity, dimensionless	0.4
Uniaxial specific storage, $cm^2\ dyn^{-1}$	2.8×10^{-5}
Calculated hydraulic diffusivity, $cm^2\ s^{-1}$	8.6

[a]Bulk material parameters are derived from initial model states.

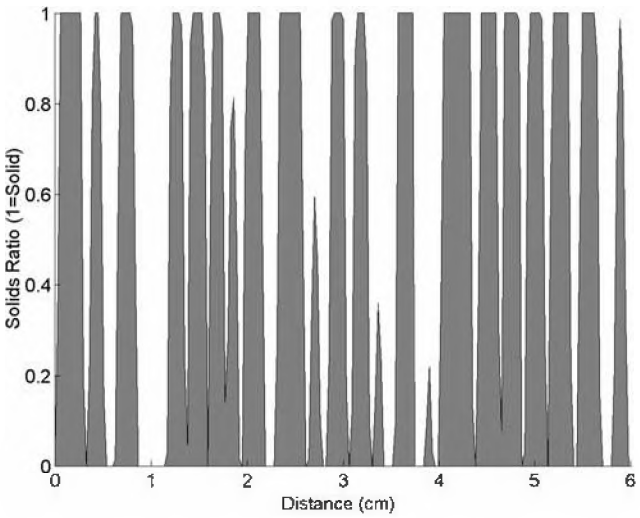

Figure 3. A 1-D map of LB fluid nodes along A-A′ (Figure 2) depicting solid ratios (gray areas are solids). When the ratio is equal to 1, that fluid node is overlain by a solid discrete element. When the solid ratio is 0 (or less than 1) that node represents pore space or some fraction of pore space.

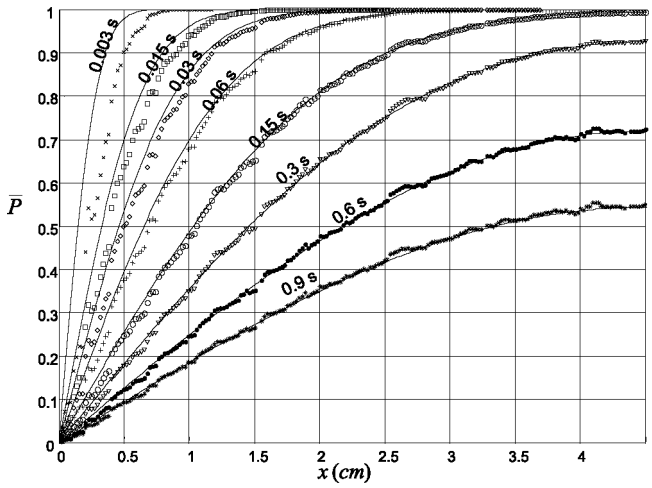

Figure 4. Plots of normalized pressure (P/P_o) versus distance for half of the LBDEM solution domain shown as different symbols for eight times. Also plotted are the analytical solutions (solid lines) at the same times using the analytical solution to the corresponding continuum media using a best fit diffusivity of 8.6 $cm^2\ s^{-1}$.

depicting solid ratios at a single point as a function of distance along the flow-parallel direction. Solid ratios refer to the percentage of solid discrete element that interacts with the Eularian fluid grid. Percent solid values plotted in Figure 3 represent the average percent solid for a column of nodes in the flow perpendicular direction. Any single cross section may be greater than 70% solid nodes (fluid nodes where solid particles lie on top). Eleven separate vertical cross sections through the model were chosen and only fluid pressure values from fluid-filled nodes (solid ratio of 0) were considered. The values were then arithmetically averaged and plotted on an x-y plot with respect to normalized pressure (P/P_o) and distance in the flow direction. The results for eight different times during the model run are illustrated for half of the domain in Figure 4. The data demonstrate diffusion-like profiles, where higher fluid pressure is forced to come into equilibrium with lower pressure boundary conditions. In each curve, especially later time curves, small inconsistencies between the smooth analytical solution and the LBDEM exist. Most likely, the heterogeneous pore body and throat size distributions are causing these deviations. Deviations are similar for results plotted at the same location but at different times, suggesting that deviations are location specific. On average, the variability is small with respect to the overall pressure magnitude.

[21] The analytical solutions (solid lines) to equation (2) are plotted on Figure 4. The analytical solution is parameterized based on the poroelasticity-based calculation of hydraulic diffusivity, 8.6 $cm^2\ s^{-1}$. A best fit result was also computed based on the sum of least squares error between the model and the analytical solution giving a similar in magnitude hydraulic diffusivity of 7.9 $cm^2\ s^{-1}$. Both values are higher than that reported by *Wang* [2000] for sandstone ($c \approx 1\ cm^2\ s^{-1}$), but not unexpected for a 2-D model with less tortuosity than would exist in a real (3-D) rock. Larger values of hydraulic diffusivity will cause fluid pressure to reach equilibrium faster. It appears that the fit between the calculated fluid pressure and the analytical solution is a strong function of time. Early time results show more deviation than the later time solutions. Larger discrepancies also exist between the solutions at the boundaries. Sources of error in the LBDEM compared to the analytical solution arise from multiple sources. In contrast to the porous medium modeled here, the analytical solution makes an assumption of a homogeneous material. The LBDEM is clearly not homogeneous at the scale at which measurements are being made. Additionally, certain assumptions in the analytical solution may not be valid near the boundaries of the model such as the possibility that in the numerical model, the hydraulic diffusivity may be a function of fluid pressure gradients, which is not captured in the analytical solution. Finally, assumptions about the 2-D nature of flow in the LBDEM model may be influencing mechanical interactions between the fluid and rock skeleton. The out of plane flow constraint, especially near the boundaries, should influence observed fluid pressure evolution in the model. Nevertheless, poroelastic predictions of diffusivity based on uncoupled model behavior correlate well with the coupled model behavior. From these results we can infer continuum parameters governing the behavior of initial model conditions.

3.3. Conceptual Model of 1-D Consolidation

[22] Consolidation of saturated porous media was first examined by *Terzaghi* [1925, 1943] and later applied to many problems in geomechanics and hydrogeology [e.g., *Domenico and Mifflin*, 1965]. In Terzaghi's formulation of 1-D consolidation, a sudden stress of σ_o is applied on the surface of a finite length fluid-saturated porous medium with an impermeable bottom boundary. The top boundary is drained, such that fluid can freely leave the consolidating porous media. This is analogous to a porous plate used in laboratory experiments of consolidation. The governing equation for this problem is identical to the fluid diffusion problem described above if the stress applied is not a function of time. This allows the pore fluid diffusion equation to be uncoupled from the mechanical equilibrium equations and results in an analytical solution that is similar to the solution of equation (2). The increase in fluid pressure due to the consolidation in the sample results in a positive pressure gradient in the direction of the drained top boundary. As fluid leaves, the system slowly returns to equilibrium. The primary parameter governing how quickly fluid escapes the porous medium is the hydraulic diffusivity, c. The analytical solution is shown in a depth vs. time plot using $c = 7.9$ in Figure 5a. Highest fluid pressure is adjacent to the bottom no-flow boundary.

3.4. Results of 1-D Consolidation With LBDEM Model

[23] Consolidation behavior of the coupled model is explored using the setup depicted in Figure 6. An assembly of approximately 1000 discs is packed into an 11 cm × 6 cm rectangular region bounded by no displacement, no flow walls. Physical properties of the discrete elements are assigned to mimic those of quartz grains (Table 1). The assembly of elements in Figure 6 is prepared identically to the model in Figure 2. Because the analytical solution uses an assumption of idealized poroelastic behavior and hence simplifies the behavior, the main test for the LBDEM model

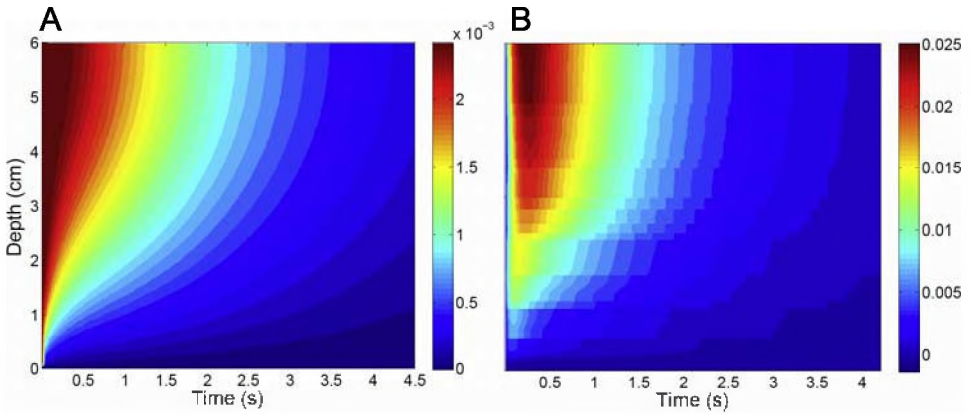

Figure 5. Contour plots of normalized fluid pressure (P/P_o) along a composite section (see text for details) parallel to applied load direction for both (a) the analytical solution and (b) the LBDEM solution for Terzaghi's consolidation problem. Analytical solution assumes ideal poroelastic response (pressure attains maximum values instantaneously). Higher fluid pressure values (red) occur adjacent to bottom (depth of 6 cm) boundary of modeled system.

is to demonstrate fluid pressurization as a result of an applied stress. The top boundary is assigned a constant applied stress with a porous discrete element such that fluid flow is not impeded. The fluid at this boundary is maintained at zero gauge pressure. The bottom and side boundaries are specified as a no-flow and no-displacement boundary. Initially, the solid framework is in equilibrium with the boundary conditions and the fluid pressure is constant throughout the assembly.

[24] The simulation begins with an application of the stress boundary condition on the drained boundary (top). In response to this condition, the assembly of cylinders consolidates and fluid pressure rises. Early time results of Figure 5b illustrate the behavior of the fluid pressure response. A comparison of the two results suggests a short lag time in the response of fluid pressure in the LBDEM simulation in the maximum fluid pressure (Figure 5b). Unlike the analytical solution (Figure 5a), which assumes an ideal poroelastic response as an initial condition, the coupled model has a finite wave speed. Therefore the response of the assembly to the new boundary condition takes time to reach the maximum fluid pressure. Experimental evidence [*Gunaratne et al.*, 1996] using a dynamically applied stress suggests that the time to reach peak fluid pressure is on the order of tenths of seconds depending on material properties, including the degree of saturation, permeability, and media compressibility [*Gunaratne et al.*, 1996; *Valliappan et al.*, 1995]. In our simulation the peak fluid pressure is reached 0.2 s after the application of the boundary stress, consistent with theory and empirical data.

4. Application of LBDEM to Natural Hydraulic Fracturing

[25] In this section we apply the LBDEM model to the problem of natural hydraulic fracturing. Natural hydraulic fractures (NHF) are fractures induced by the presence of elevated fluid pressure with respect to hydrostatic pressure. The importance and existence of NHFs in the Earth's crust has been debated for over 30 years [*Secor*, 1965], yet the conditions under which they form remain controversial. *Flekkøy et al.* [2002] present the development of a numerical model that couples a discrete spring network representation and Darcy's law to model fluid pressure induced øfractures (hydrofractures). They briefly examine two scenarios of hydrofracturing: one in which fractures result from a point source of fluid pressure and the other involves hydraulic fracturing of a cap rock. Both models suggest that pressure diffusion is important for simulating fracture growth. We apply the LBDEM model to similar problems to examine the feedbacks between fracture growth and fluid dissipation in the porous media. This is a unique problem in fracture mechanics since the presence of elevated fluid pressure and fluid flow plays a first-order role in fracture genesis. Correspondingly, the LBDEM model is ideal for studying this problem because (1) a strong coupling between fluid flow and solid deformation exists and (2)

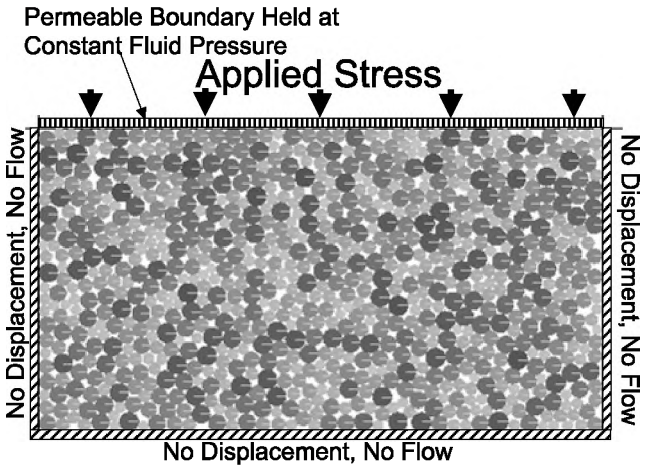

Figure 6. Conceptual model for consolidation problem identifying mechanical and fluid boundary conditions. Shading of particles is proportional to element size (darker indicates larger). Top boundary consists of a drained ($P = 0$) fluid condition with a corresponding application of applied stress. All other boundaries are no-flow and no-displacement.

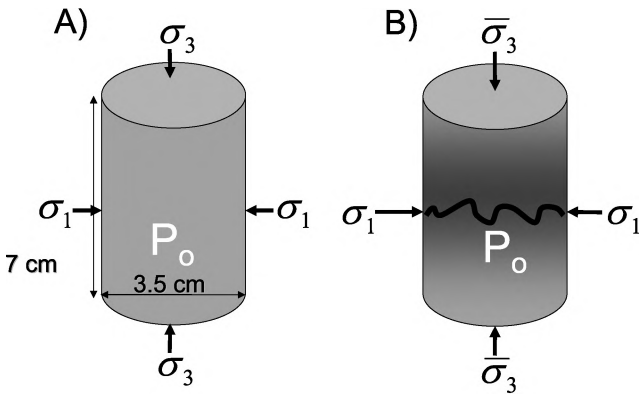

Figure 7. Initial and boundary conditions for experimental approach to generating natural hydraulic fractures. (a) Initial conditions on the modeled material. (b) Modification of the mechanical boundary conditions that marks the beginning of the test. The shading in Figure 7b reflects the fluid pressure at a short time after change in boundary condition, where the pressure is kept elevated relative to the minimum stress by the lag time that occurs as a result of fluid flow.

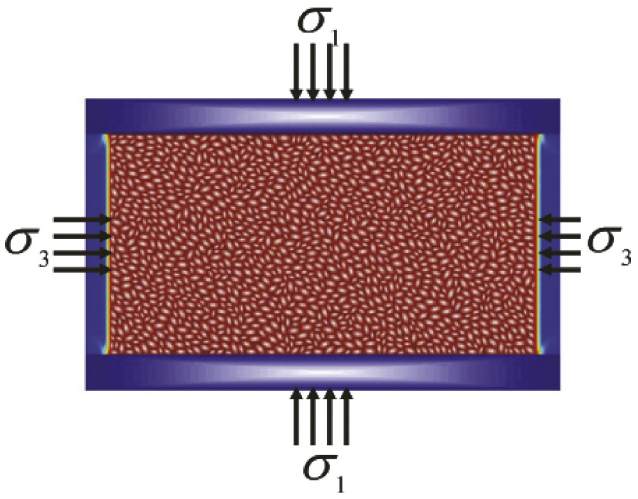

Figure 8. Base LBDEM model for NHF simulation. Approximately 1000 ellipse-shaped elements are packed into a 7 by 3.5 cm area and constrained by mechanical boundary conditions of σ_3 and σ_1. Long flat elements served to apply σ_1 while σ_3 is applied via a raft of boundary ellipse elements.

fracture initiation and propagation must be modeled to analyze the resulting fluid flow.

4.1. Test Design

[26] A new method was previously designed to generate NHFs under laboratory constraints [*Boutt*, 2004; D. Boutt et al., Genesis of natural hydraulic fractures in the laboratory, submitted to *International Journal of Rock Mechanics Abstracts*, 2007]. The test, shown in Figure 7, begins with initial conditions on a cylindrical sample of rock saturated with a fluid pressure P_o, which is typical of traditional triaxial tests with the exception that the σ_3 is axial and σ_1 laterally confines the sample. At the start of the test, both P_o and σ_3 are instantaneously lowered to P and $\overline{\sigma_3}$, respectively. The drop in both stress and fluid pressure at the boundary will create conditions conducive to the generation of extension fractures in the sample. These conditions consist of fluid pressure at the center of the sample being greater than the local axial stress which, assuming quasi-equilibrium with new boundary conditions, should be $\overline{\sigma_3}$. As a result, extension fractures should form parallel to σ_1 in areas of high P and low $\overline{\sigma_3}$. In NHFs, unlike induced hydraulic fractures, ambient fluid pressure is higher surrounding the fracture than inside the fracture itself. This condition imposes constraints on how resulting fractures initiate and interact, which is examined using the LBDEM model in section 4.2.

[27] Differing time constants governing fluid flow and mechanical equilibrium are responsible for creating a condition of high P and low σ_3 at the sample center. Specifically, the fluid diffusion time constant is much lower (i.e., slower) than the mechanical equilibrium time constant. In porous media, the time it takes for a given fluid pressure to come to equilibrium with a change in boundary conditions is a function of the rock's hydraulic diffusivity (c). As above, c has mks units of length^2/time m^2 s^{-1} and a time of L^2/c is required for a pressure change to propagate a distance L. The diffusion time is a function of the rocks hydrologic properties (k, S) and it relies on the fluid properties (ρ, μ).

4.2. LBDEM Conceptual Model

[28] A 2-D LBDEM model of 958 ellipse-shaped elements with an aspect ratio of 0.5 were packed into a 7 cm long by 3.5 cm wide box (Figure 8) to model the above experimental conditions. Ellipse-shaped elements were chosen for their superior frictional and mechanical properties compared to circular elements. Similar to a laboratory test, boundary conditions are applied to the discrete element assembly with platens (rectangular discrete elements) until a specified stress is reached.

[29] To simulate the behavior of a cohesive rock, individual discrete elements were bonded to one another. In this DEM formulation bonds are modeled as point-to-point constraints between neighboring particles using the spring formulation as

$$F_b = k_b \Delta x, \tag{5}$$

where F_b is the force in the bond, k_b is bond stiffness, and Δx is relative displacement of the neighboring particles. Bonds are aligned with the surface normals and connect the closest surfaces of the two particles of interest. If F_b is greater than or equal to the bond strength F_b^{crit} the constraint is removed and bonded elements are allowed to move

Table 2. Parameters of Solid Assembly for NHF Model

Parameter	Value
Friction, dimensionless	0.5
Element normal stiffness, dyn cm^{-1}	1×10^5
Element shear stiffness, dyn cm^{-1}	6×10^5
Element size range, cm	0.11–0.07
Bond strength F^{crit_b}, dyn	700
Bond stiffness k_b, dyn cm^{-1}	1×10^5

Table 3. Parameters of Fluid Lattice for NHF Model

Parameter	Value
Viscosity, $cm^2\ s^{-1}$	0.2
Relaxation time, dimensionless	0.625
Node spacing, cm	0.009
Fluid radius, dimensionless	0.6
Time step, s	1×10^{-5}

freely. This bonding approach has no implicit shear strength. In reality, the bond has some finite shear strength since it is modeled as a surface-to-surface contact, and any offset (normal or tangential) great enough to exceed the F_b^{crit} will cause the bond to fail. Additionally, the bond has no physical interaction with the flowing fluid. Properties of the discrete element portion of the simulations are listed in Table 2.

[30] The simulated LB fluid has a dynamic viscosity of 0.2 $cm^2\ s^{-1}$, similar to that of water (Table 3). The simulation consisted of approximately 500,000 fluid nodes. The Eularian fluid lattice, shown as the colored area in Figure 8, extends beyond the edge of the discrete elements to allow straining of the element assembly during fracturing. The sample in Figure 8 was tested under a constant fluid pressure drop and the resulting steady state discharge through the system was recorded. Resulting permeability of the model specimen was 1.3×10^{-4} cm^2 or 1.3×10^{-8} m^2. Specific properties of the fluid lattice are given in Table 3.

[31] The initial conditions for the fracturing test applied to the LBDEM model are shown in Figure 8. Initially, the sample is loaded hydrostatically to an effective stress of 50 dyn cm^{-2} (500 kPa), then the effective axial stress (sample short axis) is dropped to 40 dyn cm^{-2}, while holding the lateral stress constant. The lateral (sample long axis) stress is maintained via platens while the axial stress is applied through the discrete elements along the boundary of the model. This allows both the application of a stress and movement of fluid through the boundary. The initial fluid pressure within the sample is constant. The bond strength of the elements is 700 dyn for all models. This value is reasonable when compared to the initial fluid pressure drop across the sample, 1.7 dyn cm^{-2}. In relative terms, the bond strength is akin to a tensile strength of 7 MPa for a fluid pressure drop of ~17 MPa across the sample.

[32] The test begins with a drop in both the axial stress and fluid pressure at the boundaries. For all tests, the axial stress is dropped to 0.1 dyn cm^{-2} and the fluid pressure difference ($P_o - P$) is 1.7 dyn cm^{-2}. Fluid pressure and fluid velocity were monitored along a cross section parallel to the long axis of the model specimen. In addition, screen shots of the model were taken at 0.001 s intervals.

4.3. Natural Hydraulic Fracture Modeling Results

[33] The model (Figure 8) was executed under the conditions described above for 2 s of model time, about the time required for the system to come to a new equilibrium state. Snapshots of model state are presented in Figure 9 for early through late time model behavior (animation of

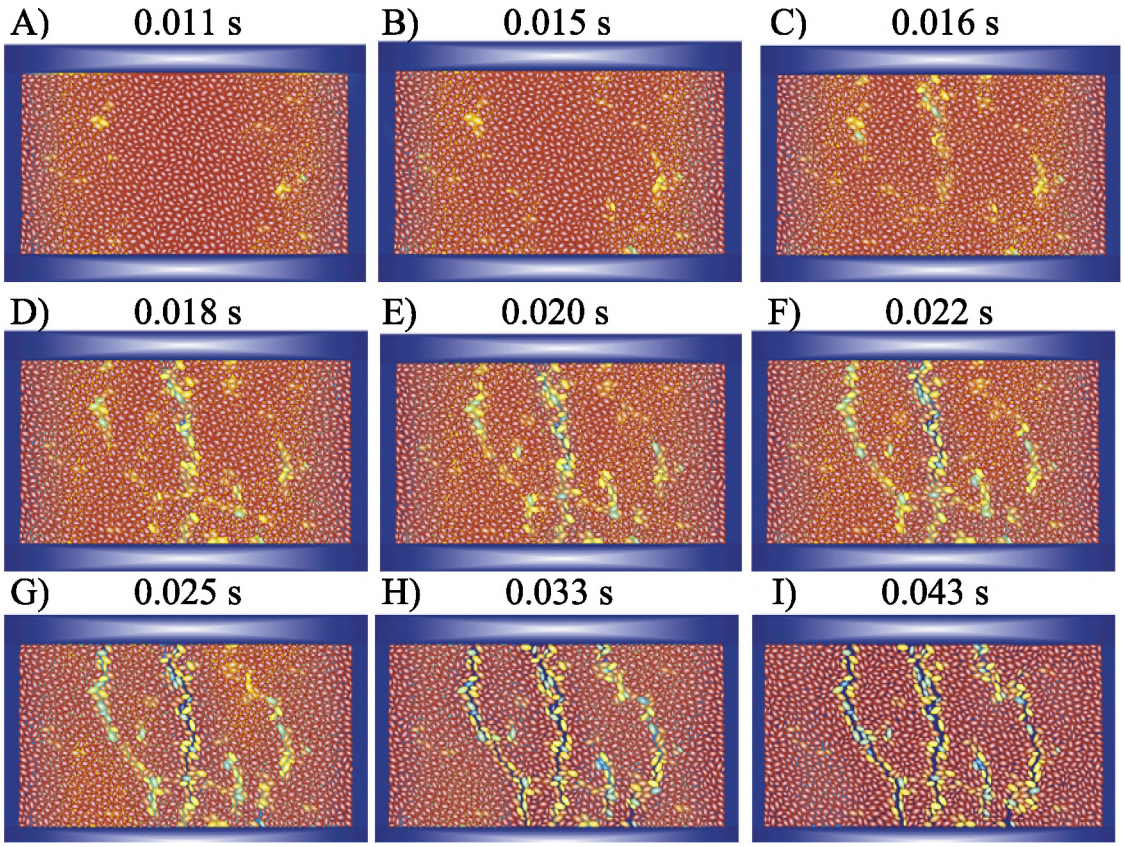

Figure 9. Time series of model states the start of the test presented in Figure 7. Element color is proportional to the percent bonds broken and color shading behind elements is fluid pressure with high fluid pressure being warm colors.

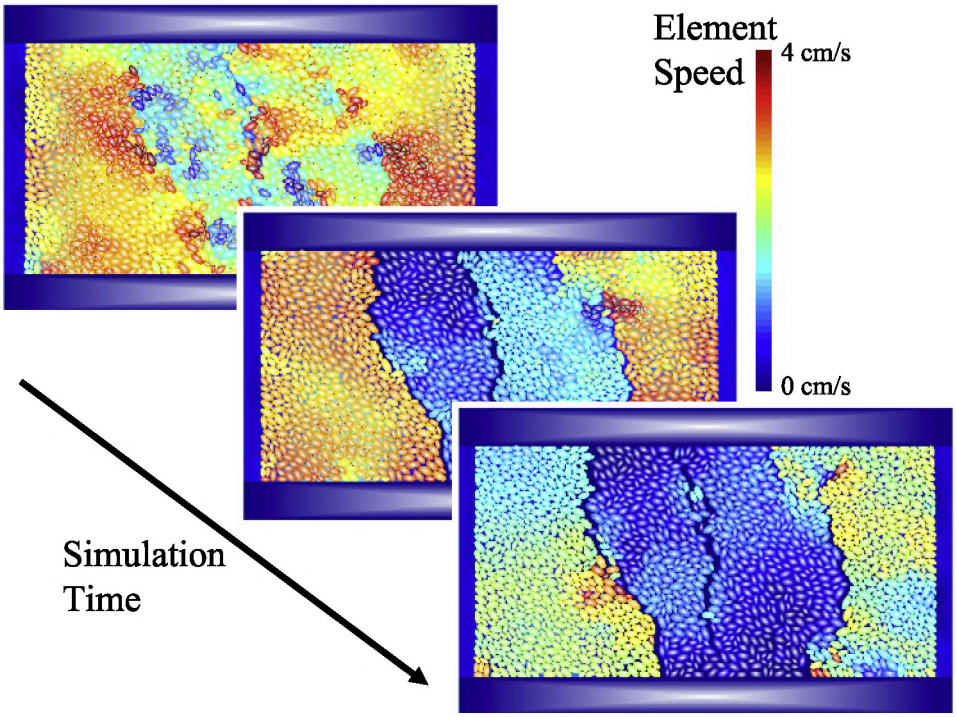

Figure 10. Colored element particle speeds for three different times during simulation. Elements with higher velocity magnitudes are colored with warmer (red) colors while blue colors indicate lower element velocity magnitudes. (top) At early time, bulking loading of fluid causes differential movement of particles (during fracture initiation) as indicated by contrast in element speed at incipient fracture location. (middle) Fractures are completely throughgoing and outside fracture blocks are moving as coherent discrete entities. (bottom) Simulation domain is approaching equilibrium with new boundary conditions.

Figure 9 is available as Animation S1 in the auxiliary material). As the axial stress is dropped on both boundaries, forces between individual elements are lowered, resulting in an overall extensional strain in the elastic framework. The additional fluid pressure drop on the boundaries cause large pressure gradients toward the ends of the discrete element assembly. The overall pressure gradient is sufficiently high to cause breakage of the element bonds. These individual bond breakages coalesce into larger macroscopic features that split the assembly parallel to the maximum stress direction. Figure 10 highlights these fractures, emphasizing element speeds, and illustrating that individual blocks within the assembly are moving as coherent groups.

[34] Test runs of dry models with identical boundary and initial conditions were performed with no resulting fractures but with less than 1% axial strain. Saturated models with no fluid pressure drop on the boundaries, but with a drop in the axial stress, also did not form fractures.

[35] The fracture growth results in Figure 9 demonstrate that bond breakages are initiated closer to the boundaries before the central fractures form. Although counterintuitive, fast wave speeds in the solid discrete element assembly cause elements near the boundaries to relieve force first, and the fluid pressure gradients then cause bond breakages. These bond breakages rarely coalesce into the larger macroscopic fractures seen in the center of the assembly. This is most likely because the pressure gradients near the boundaries drop faster than those in the middle of the model.

[36] The orientations of both the large throughgoing fractures and smaller fractures are roughly perpendicular to the minimum stress direction. This result is consistent with predictions from a Mohr circle analysis. Slight deviations in fracture orientation are local in nature and represent preferential breakage of weak bonds around stronger bonds. It appears that the preferential path of a given fracture is through areas where elements are oriented with their long axis normal (broadside) to the overall fluid pressure gradient direction. One proposed mechanism for this is because such elements have more surface area exposed to prevailing fluid pressure gradients, resulting in larger net forces on the elements. Disc-shaped elements will not exhibit this phenomenon. An additional hypothesis is that the mechanical anisotropy, induced by grain shape, could be causing this phenomenon.

[37] One important physical fracture process that the LBDEM technique can capture is fracture initiation. Continuum-based formulations require assumptions about initial crack or fracture length that limit model applicability or generality. The LBDEM method's smallest length scale (element size) has a first-order control on initial fracture length. The relative location and orientation of the elements also controls where the fractures are located (i.e., fracture spacing less than element size is not possible). Most extension fractures form along grain boundaries [*Kranz*, 1983]. Thus, if the element size is assumed to be equivalent to the grain size, this assumption is appropriate.

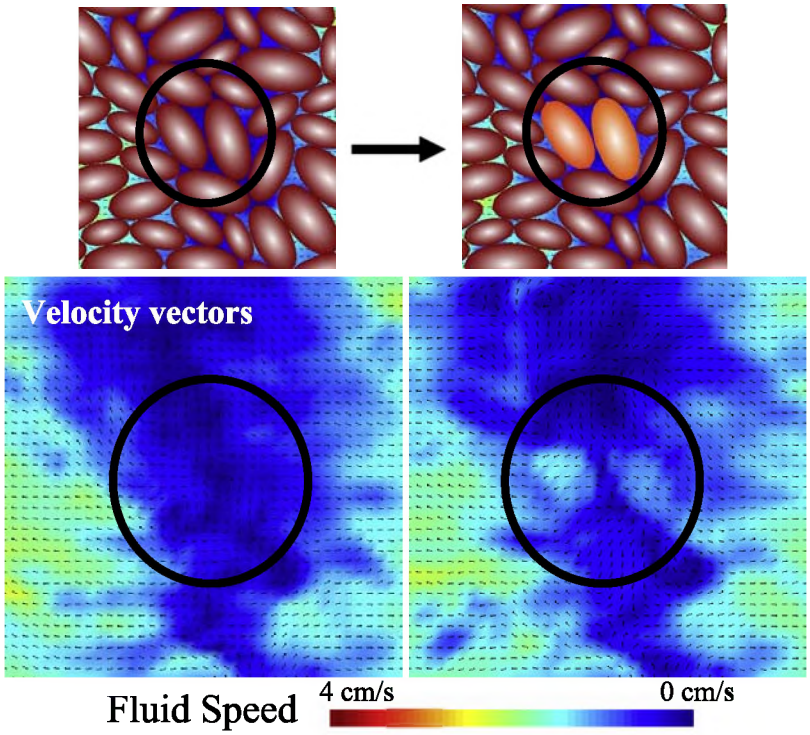

Figure 11. (top) Prebond and postbond (color particles) breakage is illustrated for a pair of particles in the central portion of the assembly. (bottom) Velocity magnitudes (dark is low velocity) and velocity vectors indicate a bulk extensional loading on the assembly. The movement of the particles induces fluid flow into the void created by the separating particles and dropping fluid pressure. Figure 11 (bottom) is of the same region indicated in Figure 11 (top) but blown up to show velocity vectors.

[38] Fluid pressure gradients develop as a result of low pressure at the boundaries and higher pressure within the system. The gradients induce interparticle stresses sufficient to break bonds. Figure 11 focuses on a particle pair central to the model in Figure 8. Prebond and postbond breakage plots are shown together with a contour plot of the fluid velocity field. These particles are being forced apart through bulk loading of fluid on the assembly. The velocity magnitudes in the prebond breakage plot of Figure 11 reveal a low-velocity zone in the vicinity of the impending bond breakage. After the bond is broken, fluid adjacent to the particles is influenced by the particle movement. The velocity vectors in the high-pressure zones on either side of the bond point in opposite directions, causing a bulk loading in the assembly, which pulls apart the two particles. Velocity vectors beneath the particles indicate extensional failure of the bond.

4.4. Fracture Propagation

[39] Propagation or growth of fractures in the LBDEM is more explicit than in an equivalent continuum model. No remeshing or damage parameters are introduced to simulate a growing fracture. Fractures are visualized as the grouping of bond breakages. An advantage to this method is that when fractures form, no modification to the fluid lattice needs to occur to handle the change in the flow properties due to fracturing.

[40] After initial bond breakage, fluid pressure drops in the newly opened fracture and causes positive fluid pressure gradients toward the fracture (Figure 9). Despite this local forcing, macroscale fluid pressure gradients are large enough to cause the particles to move apart. Figure 12 indicates that local fluid forces are not high enough to cause the bond breakage. This suggests that local-scale pressure gradients are not significant in fracture propagation at the macroscale. This distribution of pressure gives rise to fluid pressure gradients that are into and toward the fracture, yet fractures still propagate. Fluid loading on the assembly appears to be responsible for further fracture propagation. As the simulation progresses, the fractures are pulled further apart until the system returns to equilibrium. A small oscillation between fracture opening and closing in the system was observed as system energy was attenuated.

5. Model Limitations

[41] Although the generalized LBDEM coupling leads to a model that is able to capture coupled fluid-solid behavior for systems with very low concentrations of discrete elements to systems with small amounts of fluid present, the model formulation as presented above does not allow the appropriate modeling of granular porous media under certain porous media conditions. These porous media conditions include the strong compaction limit, where the available pore space for fluid to reside is reduced to very small values. One of the main reasons for this is the assumption of a two-dimensional system which has a substantially higher residual porosity than true three-dimensional sediment in a strongly compacted state. Spherical-based three-dimensional DEM models with narrow particle size

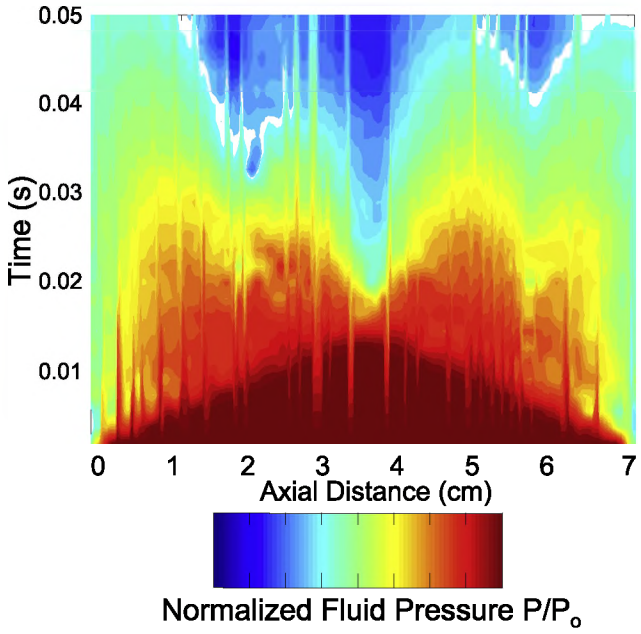

Figure 12. A contour plot of normalized fluid pressure (P/P_o) along the central axis of the model domain (parallel to σ_3) versus time since beginning of simulation. Warmer colors correspond to higher fluid pressure. As the fluid pressure is dropped on the boundaries (at time 0), the pressure within the model domain begins to drop immediately and propagates through the sample. Fractures begin to initiate at 0.16 s (see Figure 9) and serve to alter the fluid pressure distribution as fluid pressure drops within the fractures at 2 cm, 3.7 cm, and 6.1 cm. As the simulation progresses fluid pressure falls and eventually comes to equilibrium with boundary conditions.

distributions have the same troubles capturing this limit, as these models also allow an artificially large porosity under optimally packed conditions. An additional area where this model breaks down is at the lubrication limit where a small amount of fluid is compressed between two solid surfaces. The model as presented here does not allow the surfaces to get this close to one another because of the ever-present fluid gap and the stiffness of the contact between discrete elements. Regardless, the LB formulation used in this paper tends to break down when fluid gaps are equal to the grid spacing because hydrodynamic force calculations become inaccurate. For problems in which resolving the coupled dynamics in the lubrication limit is deemed important, LB force calculations can be corrected and are available from *Nguyen and Ladd* [2002].

6. Conclusions

[42] This paper presents the application of direct fluid-solid coupling scheme to the mechanics of flow through porous media. The model is built on the well-established methods of solid (DEM) and fluid (LB) mechanics. Coupling is achieved through momentum transfer from the fluid to the solid and through the enforcement of a no-slip condition at the solid/fluid interface. By handling the coupling directly, we avoid the typical assumptions of Darcy flow and effective stress and are able to model a variety of problems including strongly deforming materials.

[43] We suggest an additional way of handling discrete coupled model of poromechanics without using Darcy's law on a scale that is hard to justify. In addition to providing subcontinuum properties of porous media, this method captures continuum-scale poroelastic phenomena never before observed with a published discretely coupled model.

[44] LBDEM models were developed that enable the comparison of 1-D analytical solutions for fluid flow in slightly compressible porous media. The results from this comparison indicate that the LBDEM achieves a good match with the analytical solution. Deviations between the continuum theory and our pore-scale models are most likely the result of (1) the 2-D nature of the model (hydraulic radius approximation) and (2) the fact that our model captures subrepresentative elementary volume behavior that is smeared in continuum representations. In addition, the hydraulic diffusivity of the model is slightly larger than that expected in a similar geologic material. This is due to the fact that the modeled medium comprises relatively few particles with the resulting permeability higher than the equivalent geologic material.

[45] The consolidation of saturated porous media showed the dynamic and poroelastic response of the LBDEM model. Given that we are solving the fully dynamic equations of motion for both the fluid and solid, direct comparisons with instantaneous undrained responses are not possible. Nevertheless, the model qualitatively captures consolidation behavior, for both initial pressurization and fluid flow out of the domain.

[46] Modeling of natural hydraulic fractures using the coupled LBDEM provided unique insight into the initiation and propagation of fractures in a system where a strong coupling between fluid flow, fluid pressure, and solid mechanics exists. Numerous tensile fractures parallel to the maximum stress direction were generated in the models. The coupled evolution of the system indicated that fluid pressure in the fractures actually drops below pressure in the surrounding media, causing localized fluid flow into the fractures.

[47] **Acknowledgments.** This research was funded in part by the U.S. Department of Energy through the Natural Gas and Oil Technology Partnership. Sandia is a multiprogram laboratory operated by Sandia Corporation, a Lockheed Martin Company, for the U.S. Department of Energy under contract DE-AC04-94AL85000.

References

Boutt, D. F. (2004), Discrete analysis of the role of pore fluids in the genesis of opening mode fractures in the shallow crust, Doctoral dissertation, N. M. Inst. of Min. and Technol., Socorro.

Boutt, D. F., and B. J. O. L. McPherson (2002), Simulation of sedimentary rock deformation: Lab-scale model calibration and parameterization, *Geophys. Res. Lett.*, *29*(4), 1054, doi:10.1029/2001GL013987.

Boutt, D. F., B. K. Cook, B. J. McPherson, and J. Williams (2003), Application of a directly coupled numerical model of fluid-solid mechanics, in *Soil and Rock America 2003*, edited by T. Culligan, A. Whittle, and H. Einstein, pp. 977–983, Mass. Inst. of Technol., Cambridge.

Bruno, M. (1994), Micromechanics of stress-induced permeability anisotropy and damage in sedimentary rock, *Mech. Mater.*, *18*, 31–48.

Bruno, M., and R. Nelson (1991), Microstructural analysis of the inelastic behavior of sedimentary rock, *Mech. Mater.*, *12*, 95–118.

Campbell, C., P. Cleary, and M. Hopkins (1995), Large scale landslide simulations: Global deformation, velocities and basal friction, *J. Geophys. Res.*, *100*, 8267–8383.

Carslaw, H., and J. Jaeger (1959), *Conduction of Heat in Solids*, 2nd ed., Clarendon, Oxford, U. K.

Chen, S., and G. Doolen (1998), Lattice-Boltzman. method for fluid-flows, *Annu. Rev. Fluid Mech.*, *20*, 329–364.

Cleary, P. W., and C. S. Campbell (1993), Self-lubrication for long runout landslides: Examination by computer simulation, *J. Geophys. Res.*, *98*(B12), 21,911–21,924.

Cook, B. K. (2001), A numerical framework for the direct simulation of solid-fluid systems, Doctoral dissertation, Mass. Inst. of Technol., Cambridge.

Cook, B. K., D. Noble, D. Preece, and J. Williams (2000), Direct simulation of particle laden fluids, in *Fourth North American Rock Mechanics Symposium*, pp. 279–286, A. A. Balkema, Rotterdam, Netherlands.

Cook, B. K., D. Noble, and J. Williams (2004), A direct simulation method for particle-fluid systems, *Eng. Comput.*, *21*, 151–168.

Cundall, P. (1971), A computer model for simulating progressive, large-scale movement in block rock systems, in *Rock Fracture*, vol. 1, Int. Soc. for Rock Mech., Lisbon, Portugal.

Cundall, P., and O. Strack (1979), A discrete element model for granular assemblies, *Geotechnique*, *29*(1), 47–65.

Cundall, P., A. Drescher, and O. Strack (1982), Numerical experiments on granular assemblies: Measurements and observations, in *Deformation and Failure of Granular Materials*, edited by J. Jenkins and H. Luger, pp. 355–370, A. A. Balkema, Brookfield, Vt.

Domenico, P., and M. Mifflin (1965), Water from low permeability sediments and land subsidence, *Water Resour Res.*, *4*, 563–576.

Flekkøy, E. G., A. Malthe-Sørenssen, and B. Jamtveit (2002), Modeling hydrofracture, *J. Geophys. Res.*, *107*(B8), 2151, doi:10.1029/2000JB000132.

Green, D., and H. Wang (1990), Specific storage as a poroelastic coefficient, *Water Resour Res.*, *26*, 1631–1637.

Gunaratne, M., M. Ranganath, S. Thilakasiri, G. Mullins, P. Stinnette, and C. Kuo (1996), Study of pore pressures induced in laboratory dynamic consolidation, *Comput. Geotech.*, *18*(2), 127–143.

Hazzard, J., P. F. Young, and S. Maxwell (2000), Micromechanical modeling of cracking and failure in brittle rocks, *J. Geophys. Res.*, *105*, 16,683–16,697.

Helm, D. C. (1994), Horizontal aquifer movement in a Theis-Thiem confined system, *Water Resour Res.*, *30*, 953–964.

Kranz, R. L. (1983), Microcracks in rocks: A review, *Tectonophysics*, *100*, 449–480.

Li, L., and R. Holt (2001), Simulation of flow in sandstone with fluid coupled particle model, in *Proceedings of the 38th U. S. Rock Mechanics Symposium: Rock Mechanics in the National Interest*, edited by D. Elsworth, J. P. Tinucci, and A. Heasley, pp. 511–516, A. A. Balkema, Rotterdam, Netherlands.

McPherson, B., and J. Bredehoeft (2001), Overpressures in the Uinta basin, Utah: Analysis using a three-dimensional basin evolution model, *Water Resour Res.*, *37*, 857–872.

Morgan, J. (1999), Numerical simulations of granular shear zones using the distinct element method 2. Effects of particle size distribution and interparticle friction on mechanical behavior, *J. Geophys. Res.*, *104*, 2721–2732.

Morgan, J., and M. Boettcher (1999), Numerical simulations of granular shear zones using the distinct element method: 1. Shear zone kinematics and the micromechanics of localization, *J. Geophys. Res.*, *104*, 2703–2719.

Neuzil, C. (1995), Abnormal pressures as hydrodynamic phenomena, *Am. J. Science*, *295*, 742–786.

Neuzil, C. E. (2003), Hydromechanical coupling in geologic processes, *Hydrogeol. J.*, *11*(1), 41–83.

Nguyen, N.-Q., and A. Ladd (2002), Lubrication corrections for lattice-Boltzmann simulations for particle suspensions, *Phys. Rev. E*, *66*, doi:10.1103/PhysRevE.66.046708.

O'Connor, R., J. Torczynski, D. Preece, J. Klosek, and J. Williams (1997), Discrete element modeling of sand production, *Int. J. Rock Mech. Sci.*, *34*(3–4), 231.

Pande, G., G. Beer, and J. Williams (1990), *Numerical Modeling in Rock Mechanics*, John Wiley, New York.

Potyondy, D. O., and P. A. Cundall (2004), A bonded-particle model for rock, *Int. J. Rock Mech. Min. Sci.*, *41*(8), 1329–1364.

Potyondy, D. O., P. A. Cundall, and C. Lee (1996), Modeling rock using bonded assemblies of circular particles, in *Rock Mechanics: Tools and Techniques: Second North American Rock Mechanics Symposium (NARMS)*, edited by M. Aubertinin, F. Hassani, and H. Mitri, pp. 1937–1944, A. A. Balkema, Rotterdam, Netherlands.

Rege, N. (1996), Computational modeling of granular materials, Doctoral dissertation, Mass. Inst. of Technol., Cambridge.

Secor, D. T. (1965), Role of fluid pressure in jointing, *Am. J. Sci.*, *263*, 633–646.

Terzaghi, K. (1925), *Erdbaumechanik auf Bodenphysikalischer Grundlage*, Deuticke, Leipzig, Germany.

Terzaghi, K. (1943), *Theoretical Soil Mechanics*, John Wiley, New York.

Valliappan, S., J. Yazdi, and C. Zhao (1995), Analytical solution for two-dimensional dynamic consolidation in frequency domain, *Int. J. Numer Anal. Methods Geomech.*, *19*, 663–682.

Wang, H. (2000), *Theory of Linear Poroelasticity: With Applications to Geomechanics and Hydrogeology*, Princeton Univ. Press, Princeton, N. J.

Williams, J. R., and N. Rege (1997), The development of circulation cell structures in granular materials undergoing compression, *Powder Technol.*, *90*, 187–194.

Yow, J., and J. Hunt (2002), Coupled processes in rock mass performance with emphasis on nuclear waste isolation, *Int. J. Rock Mech. Min. Sci.*, *39*, 143–1150.

D. F. Boutt, Department of Geosciences, University of Massachusetts Amherst, 233 Morrill Science Center, 611 N. Pleasant St., Amherst, MA 01003, USA. (dboutt@geo.umass.edu)

B. K. Cook, Infrastructure and Information Technology, Sandia National Laboratories, P.O. Box 5800, MS 0576, Albuquerque, NM, USA.

B. J. O. L. McPherson, Department of Civil and Environmental Engineering, University of Utah, 122 South Central Campus Drive, 104 CME, Salt Lake City, Utah 84112-0561, USA.

J. R. Williams, Department of Civil and Environmental Engineering, MIT, Room 1-250, 77 Massachusetts Avenue Cambridge, MA 02139, USA.